

LA-UR-16-23200

Approved for public release; distribution is unlimited.

Title: Evaluation of the Pool Critical Assembly Benchmark with Explicitly-Modeled Geometry using MCNP6

Author(s): Joel A. Kulesza
Roger L. Martz

Intended For: Nuclear Technology

Issued: 2016-05-06



Disclaimer: Los Alamos National Laboratory, an affirmative action/equal opportunity employer, is operated by the Los Alamos National Security, LLC for the National Nuclear Security Administration of the U.S. Department of Energy under contract DE-AC52-06NA25396. By approving this article, the publisher recognizes that the U.S. Government retains nonexclusive, royalty-free license to publish or reproduce the published form of this contribution, or to allow others to do so, for U.S. Government purposes. Los Alamos National Laboratory requests that the publisher identify this article as work performed under the auspices of the U.S. Department of Energy. Los Alamos National Laboratory strongly supports academic freedom and a researcher's right to publish; as an institution, however, the Laboratory does not endorse the viewpoint of a publication or guarantee its technical correctness.

Abstract

Despite being one of the most widely used benchmarks for qualifying light water reactor (LWR) radiation transport methods and data, no benchmark calculation of the Oak Ridge National Laboratory (ORNL) Pool Critical Assembly (PCA) pressure vessel wall benchmark facility (PVWBF) using MCNP6 with explicitly-modeled core geometry exists. As such, this paper provides results for such an analysis. First, a criticality calculation is used to construct the fixed source term. Next, ADVANTG-generated variance reduction parameters are used within the final MCNP6 fixed source calculations. These calculations provide unadjusted dosimetry results using three sets of dosimetry reaction cross sections of varying ages (those packaged with MCNP6, from the IRDF-2002 multi-group library, and from the ACE-formatted IRDFF v1.05 library). These results are then compared to two different sets of measured reaction rates. The comparison agrees in an overall sense within 2% and on a specific reaction- and dosimetry location-basis within 5%. Except for the neptunium dosimetry, the individual foil raw calculation-to-experiment comparisons usually agree within 10% but is typically greater than unity. Finally, in the course of developing these calculations, geometry that has previously not been completely specified is provided herein for the convenience of future analysts.

Keywords

Pool Critical Assembly (PCA); MCNP6; Pressure Vessel Benchmark

I. Introduction

This paper provides results for an analysis of the Oak Ridge National Laboratory (ORNL) Pool Critical Assembly (PCA) pressure vessel wall benchmark facility (PVWBF) with explicitly-modeled core geometry using MCNP6. The ORNL PCA PVWBF is one of the most widely used benchmarks for qualifying light water reactor (LWR) radiation transport methods and data. Since its publication in 1997, Reference 1 has provided a well-defined neutron source, material compositions, and geometry to calculate reaction rates at various positions external to the PCA core to compare against measured reaction rates.

The PCA benchmark report, Reference 1, used several discrete ordinates DORT (Ref. 2) calculations with homogenized fuel regions to calculate 2D neutron flux solutions that were synthesized with DOTSYN (Ref. 3) to develop 3D solutions. These 3D solutions were then folded with dosimetry reaction cross sections. In addition, various full 3D calculations have been performed with codes such as THREEDANT (Refs. 4, 5), MCNP3A (Refs. 4, 6), TORT (Refs. 7, 8, 9), RAPTOR-M3G (Refs. 10, 11), and PENTRAN (Refs. 12, 13). However, all of these analyses also used homogenization within the core region. Reference 14 compared results using both homogenized and explicit core geometry with TRANSFX (Ref. 15). Recent analyses (Refs. 16, 17, 18) performed 3D Monte Carlo calculations with explicit core geometry with KENO and Monaco from the SCALE 6 suite of analysis codes (Ref. 19) and TRIPOLI (Ref. 20). Note that Reference 17 approximated the fuel plates as flat whereas References 16, 18 modeled the curved fuel plates exactly. Regardless, until now no MCNP[®] calculation has been performed with explicitly-modeled core geometry. In this analysis, MCNP6's constructive solid geometry (CSG) capability is used to construct the model geometry. Exercising MCNP6's unstructured mesh (UM) geometry system is left as future work.

This paper briefly describes the PCA experimental configuration and MCNP6 model geometry at two levels of model detail. It then details the calculational process which includes explicitly calculating the fixed source term based on a criticality calculation, retrieving appropriate dosimetry reaction cross sections, generating variance reduction parameters, and performing the final fixed source calculations. Finally, the results are presented which allow a comparison between the calculations herein and two sets of experimental values as well as between dosimetry reaction cross sections packaged with MCNP6 (Ref. 21), those available from the IRDF-2002 multi-group library (Ref. 22), and those provided with the ACE-formatted IRDFF v1.05

library (Ref. 23). In addition, explicit control and regulating rod geometry specifications are given in an appendix to provide a consistent basis for future explicit modeling efforts.

II. Experiment Description & Model Geometry

The PCA reactor core consists of 5×5 assemblies (each assembly square with approximately 8-cm sides and an active fuel region approximately 60 cm long) consisting of slightly curved highly-enriched (93%) uranium fuel plates encapsulated within aluminum. Typical assemblies have 18 fuel plates. Additional core geometry details are omitted here because they are available in Reference 1. However, note that four assemblies house either one of three B_4C -based control rods or a stainless steel 347 regulating rod. Reference 1 does not provide explicit geometric details for the control or regulating rods. The dimensions used for the analysis herein (Ref. 24) are provided in Appendix A for the convenience of future analysts.

The PCA PVWBF is reconfigurable to examine different ex-core component arrangements. Ex-core components include an aluminum core face simulator adjacent to the core and, moving radially outward, a stainless steel thermal shield, carbon steel pressure vessel simulator, and thin-walled aluminum air-filled box. The most commonly analyzed configuration (and the one analyzed herein) is the “12/13” configuration indicating that the water gaps between the core face simulator and thermal shield and between the thermal shield and pressure vessel are 12 and 13 cm, respectively. This arrangement is usually chosen because it most-closely approximates the spacing found in commercial LWRs. Regardless, within these components and the water gaps between them, aluminum experiment tubes (labeled A1–A8, B3, B5) are situated which contain dosimeters at the core midplane elevation and are otherwise filled with surrogate material to minimize perturbing the flux near the dosimetry. Traditionally, results are reported for six dosimetry reactions:

- $^{27}\text{Al} (n, \alpha) ^{23}\text{Na}$,
- $^{58}\text{Ni} (n, p) ^{58}\text{Co}$,
- $^{103}\text{Rh} (n, n') ^{103m}\text{Rh}$,
- $^{115}\text{In} (n, n') ^{115m}\text{In}$,
- $^{238}\text{U} (n, f) ^{137}\text{Cs}$, and
- $^{237}\text{Np} (n, f) ^{137}\text{Cs}$

at dosimetry positions A1–A7. As such, those are the reactions and positions analyzed herein. Figure 1 shows a plan view of the model geometry. Only the dosimetry positions analyzed herein (A1–A7) are labeled to avoid obscuring the figure. Figure 2 shows a detailed plan view of a control rod which also illustrates the curvature of the fuel and inter-assembly gaps. Figure 3 shows the six multi-group dosimetry reaction cross sections from IRDF-2002 to illustrate the range of energies surveilled (with between 169 and 641 groups used for a given reaction).

In order to perform the calculations herein, two geometry models are used. First, a detailed model is constructed using the geometry and material information from References 1, 24 to model all dimensions and materials explicitly (as shown in Figures 1 and 2). This detailed model is used for performing the criticality calculations to define the fixed source term and then ultimately the fixed source calculations. Next, a model with simplified core geometry is created to enable automated variance reduction with ADVANTG (Ref. 25). The primary difference between the detailed and simplified model is that the simplified core region contains 5×5 cells of smeared materials in the core region (with one cell per fuel assembly) and is therefore not shown. The simplified model is created for two reasons. First, it alleviates the material smearing burden that ADVANTG would otherwise bear by manually smearing each assembly with the material given in Table 2.1 of Reference 12. If the smearing operations are left to ADVANTG, performance degradation and sporadic instability are observed. Also, the simple models explicitly include dosimetry reaction cross sections as tally response modifiers (using the MCNP[®] `e0/em0` cards) because ADVANTG cannot use reactions specified as tally multipliers provided directly by nuclear data files (with the MCNP[®] `fm` card). More detail regarding the application of ADVANTG to generate variance reduction parameters is given in Section III.B. Following the ADVANTG executions, fixed source calculations are executed using the detailed model to directly obtain the desired reaction rates.

III. Computational Process

Each of the MCNP[®] calculations use a consistent “bleeding edge” (i.e., nightly-build) version of MCNP6, version 6.1.2. The latest nuclear data libraries supplied with MCNP6 are used. All MCNP[®] calculations use the default library for each material’s constituent isotope. The criticality calculation uses 250 batches of

neutrons (with the first 50 batches discarded) with 10,000 neutrons per batch. The fixed source calculations use 30 million histories.

III.A. Criticality Calculation To Determine Fixed Source Distribution

Reference 1 provides radial and axial relative power density distributions to construct a fixed source term intended for use with smeared fuel assemblies. Because this calculation uses explicit geometry, MCNP6's internal ability to generate fixed source points from a pair of criticality calculations is used instead. The general process is as follows:

1. Perform an initial criticality calculation to calculate a converged source term using the detailed geometry model shown in Figure 1. In this case, the final calculated effective eigenvalue is $0.99938 \pm 0.00059 (1\sigma)$ which is sufficiently close to critical for the purposes herein to believe that the explicit core geometry and material arrangements are specified correctly. Furthermore, this calculation passes the Shannon entropy check within MCNP6 (neutron cycle 11 is the first cycle having fission source entropy within one standard deviation of the average entropy of the last half of the cycles calculated) while the first 50 cycles are discarded.
2. Perform a second "criticality calculation" that merely reads the automatically created source tape file from the earlier calculation (containing criticality source term information) and writes a source (with the `ssw` card) for each of the fuel-bearing geometry cells. The effect of this is to write a file containing source points within each of the fuel-bearing cells suitable for use in a fixed source calculation (by default, named `wssa`). Note that this process re-uses MCNP's surface source write/read functionality where, in the special case of geometry cells that contain fissile material, rather than points on a surface the source locations are distributed throughout one or more fissile volumes.

The `wssa` file is created with 40 million source points to ensure that none are reused in the final fixed source calculations.

III.B. Generation of Variance Reduction Parameters

Next, dosimetry reaction cross sections are retrieved from the IRDF-2002 multi-group library using JANIS (Ref. 26) for the six reactions of interest. The data for each reaction is exported from JANIS, converted from an eV-based to MeV-based energy mesh (to be consistent with MCNP6), and formatted into multi-column tally response multiplier inputs (`e0/em0` cards) which are appended to six separate MCNP[®] input files, one for each reaction (which are otherwise identical). In all cases, the group structure used in IRDF-2002 is maintained in the MCNP[®] input files. Six separate files are used because of the variation in the energy response of the six reactions: minimizing the tally variance for all reactions at all detector positions concurrently gives substantially worse performance than doing so for each reaction individually. This behavior is particularly driven by the $^{27}\text{Al}(n, \alpha)^{23}\text{Na}$ reaction which has a threshold energy of about 6.5 MeV. Regardless, each of the preceding six input files (using the simplified model geometry) are executed with ADVANTG to generate mesh-based energy-dependent weight windows. All ADVANTG calculations use P_1 scattering, 2 polar, and 2 azimuthal directions with a pre-packaged ANISN-formatted library with 27 neutron groups and 19 photon groups (Ref. 27). In all cases, the ADVANTG x spatial mesh runs from -150 cm to +150 cm, the y spatial mesh runs from -100 cm to +100 cm, and the z mesh runs from -100 cm to +150 cm with 50 mesh intervals in each of the three cardinal directions and completely encompasses the MCNP[®] model geometry. ADVANTG is executed using the FW-CADIS methodology to attempt to uniformly reduce the variance for the given reaction in the input file at each of the seven dosimetry locations (i.e., A1–A7). As a result, six mesh-based weight window files are generated (one for each reaction).

III.C. Final Fixed Source Calculations

Using the six mesh-based weight window files generated by ADVANTG, MCNP6 is executed using the detailed geometry model in three configurations: using MCNP6's pre-packaged dosimetry reaction cross sections specified with the `fm` card, using the multi-group dosimetry reaction cross sections from IRDF-2002 specified on the `e0/em0` cards, and using IRDFF v1.05 dosimetry reaction cross sections loaded with the `xsN` card and specified with the `fm` card. When using MCNP6's pre-packaged data, the $^{58}\text{Ni}(n, p)^{58}\text{Co}$ and $^{115}\text{In}(n, n')^{115\text{m}}\text{In}$ reactions are from the ENDF/B-V-based 532DOS library and the remaining four reactions

are from the LLNL-evaluated ACTL/LLLDOS library. Because of the need for distinct weight windows for each reaction, a total of 18 fixed-source calculations are executed from which results are compiled.

Each of the MCNP6 executions use two types of tallies: track-length (F4) and point detector (F5). The F4 tallies are over a sphere with a radius of 1 cm centered within the experiment tubes at the core midplane elevation. Each F5 detector is centered within the associated F4 tally region. The F4 tallies are used to validate the F5 results (where all F4 and F5 results agree within 2σ with one exception and usually within 1σ). As such, the F5 results are presented herein because of the consistently lower uncertainties relative to the F4 results (which have uncertainties less than 8% (1σ) and usually less than 2%). In all cases, no spectral adjustment methods are applied; all results are compared directly with the measured normalized reaction rates.

IV. Calculation Results

The results of this work are compared to the experimental results reported in Ref. 7 directly. To provide a consistent basis for comparison between this work and Ref. 1, dosimetry reaction rates normalized per source neutron are calculated as

$$R_x = \phi \cdot \bar{\Sigma}_x \cdot 10^{-3} \cdot 10^{-24} \quad (1)$$

where

R_x is the normalized dosimetry reaction rate for reaction x [s^{-1}],

ϕ is the fission-equivalent flux from Table 1.6 of Ref. 1 [$\text{cm}^{-2}\cdot\text{s}^{-1}$],

$\bar{\Sigma}_x$ is the reaction cross section for reaction x averaged over the ^{235}U fission spectrum from Table 1.6 of Ref. 1 [mb], and

$10^{-3}, 10^{-24}$ are scaling factors [$\text{b}\cdot\text{mb}^{-1}$] and [$\text{cm}^2\cdot\text{b}^{-1}$], respectively.

The resulting dosimetry reaction rates are shown in Table I. Note that Table I gives combined uncertainties for fissile reactions and only experimental precision uncertainties for the remaining reactions which include foil size corrections, counting statistics, dead time, pileup and background corrections, corrections for interfering

reactions, run-to-run monitoring, and positional uncertainties for a given experiment position (combined uncertainties for these remaining reactions are all 6.0%). Because some reaction rate results are missing in Reference 1 a separate set of experimental results are reproduced from Reference 7 in Table II (which gives combined uncertainties for all reactions) to form a second basis for comparison. Regardless, unadjusted reaction rate results from the fixed source MCNP6 calculations using MCNP6's pre-packaged dosimetry reaction cross sections are shown in Table III, results using IRDF-2002 multi-group dosimetry reaction cross sections are shown in Table IV, and results using IRDFF v1.05 dosimetry reaction cross sections are shown in Table V. Uncertainties are given for all calculated values in Tables III–V which can be propagated by the interested reader.

Finally, calculation-to-experiment ratios (C/E) are given in Tables VI–XI. Averages are calculated by position, by reaction, and overall to describe behavior on a spatial (location-wise), energy (reaction-wise), and overall basis. This allows trends to be observed in several ways and more clearly than if the results were given without any averages calculated. Location- and energy-wise trends could not be easily observed if an overall average was the only value provided.

In all cases, the overall average C/E ratio is 1.04–1.06 suggesting that the calculation is slightly over-predicting the reaction rates, on the average, at all positions. The two positions that disagree the most are A3 and A7, both predominantly because of the disagreement of the neptunium reaction C/E ratio. Regardless, the agreement between calculation and measurements observed herein are well within the accepted uncertainties of the radiation metrology community (typically $\pm 20\%$ such as prescribed in Reference 28).

Comparing the dosimetry reaction cross sections packaged with MCNP6 and those provided by IRDF-2002 and IRDFF v.105, there is on average $\sim 1\text{--}2\%$ difference overall. In addition, each position and reaction (with the exception of $^{58}\text{Ni}(n, p)^{58}\text{Co}$ and $^{115}\text{In}(n, n')^{115\text{m}}\text{In}$) show an $\sim 1\text{--}2\%$ difference. For $^{58}\text{Ni}(n, p)^{58}\text{Co}$ and $^{115}\text{In}(n, n')^{115\text{m}}\text{In}$, the C/E ratio is $\sim 4\text{--}5\%$ higher at all dosimetry positions when compared to References 1, 7. As described previously, these data come from a different dosimetry library than the other four reactions. As such, the IRDF-2002 and IRDFF v1.05 results appear to agree within $\sim 1\text{--}2\%$ with the LLLDOS/ACTL results but there is a $\sim 4\text{--}5\%$ discrepancy between the IRDF-2002 and IRDFF v1.05 and 532DOS results.

V. Conclusions

All results presented herein agree well (generally within 5%) and are within the accepted range of the radiation metrology community (generally within 20%). As such, we have shown MCNP6 to be a suitable tool for reactor dosimetry analyses using explicitly-modeled CSG geometry with an application-specific source term. We have also performed a comparison between MCNP6's packaged dosimetry libraries, IRDF-2002, and IRDFF v1.05; showing agreement within ~5% and for the most part within ~2%. However, based upon the results herein, care should be taken when using the 532DOS library with MCNP6 because it exhibits greater differences with IRDF-2002 and IRDFF v1.05 than the LLLDOS/ACTL library. Finally, we have determined and documented the regulating and control rod geometry used herein as an aid to future analysts.

Future work includes a material sensitivity study using the model developed herein. This study would be helpful in understanding the consistently high calculated results versus the measured reaction rates at each of the dosimetry locations. Higher calculated values suggest that either the source term is flawed (unlikely because of the validation provided by the eigenvalue calculation) or there is inadequate attenuation between the source and dosimetry positions. Thus, the density and composition of excore components will be varied to assess the effect on the calculated reaction rates. In addition, no (deterministic or Monte Carlo) unstructured mesh (UM) analysis has been conducted for the PCA PVWBF so performing such an analysis with MCNP6's UM capability would be of interest. In terms of criticality analyses, it would be interesting to use the explicit geometry herein to perform approach-to-criticality calculations to compare against the PCA operational behavior.

Acknowledgements

The authors wish to thank Joel M. Risner and Bruce W. Patton of Oak Ridge National Laboratory for providing electronic reference calculations that enabled us to obtain and confirm component dimension information.

VI. References

- [1] I. Remic and F. B. K. Kam, “Pool Critical Assembly Pressure Vessel Facility Benchmark,” Tech. Rep. NUREG/CR-6454 (ORNL/TM-13205), Oak Ridge National Laboratory, Oak Ridge, TN, USA, 1997.
- [2] “TORT-DORT Two- and Three-Dimensional Discrete Ordinates Transport Version 2.8.14, RSICC Computer Code Collection CCC-543. Oak Ridge National Laboratory. Oak Ridge, TN, USA. March 1994.”
- [3] M. L. Williams, P. Chowdhury, and B. L. Broadhead, “DOTSYN: A Module for Synthesizing Three-Dimensional Fluxes in the LEPRICON Computer Code System, RSICC Peripheral Shielding Routine PSR-277. Oak Ridge National Laboratory. Oak Ridge, TN, USA. March 1990.”
- [4] W. T. Urban *et. al.*, “Pool Critical Assembly Benchmark Solutions Using MCNP and THREEDANT,” in *Reactor Dosimetry* (H. Farrar IV, E. P. Lippincott, J. G. Williams, and D. W. Vehar, eds.), (West Conshohocken, PA, USA), pp. 376–383, American Society for Testing and Materials, 1994.
- [5] Deterministic Transport Team, ““ONEDANT, TWODANT, TWOHEX, THREEDANT, TWODANT/GQ Code System Documentation”, Los Alamos National Laboratory, Los Alamos, NM, USA.”
- [6] J. T. Goorley *et. al.*, “Initial MCNP6 Release Overview — MCNP6 version 1.0,” Tech. Rep. LA-UR-13-22934, Los Alamos National Laboratory, Los Alamos, NM, USA, 2013.
- [7] A. H. Fero, S. L. Anderson, and G. K. Roberts, “Analysis of the ORNL PCA Benchmark Using TORT and BUGLE-96,” in *Reactor Dosimetry: Radiation Metrology and Assessment* (J. G. Williams, D. W. Vehar, F. H. Ruddy, and D. M. Gilliam, eds.), (West Conshohocken, PA, USA), pp. 360–366, American Society for Testing and Materials, 2001.
- [8] F. A. Alpan, “A Broad-Group Cross-Section Library Based on ENDF/B-VII.0 for Fast Neutron Dosimetry Using the CPXSD Methodology,” *Journal of ASTM International*, vol. 9, May 2012.
- [9] W. A. Rhoades and D. B. Simpson, “The TORT Three-Dimensional Discrete Ordinates Neutron/Photon Transport Code,” Tech. Rep. ORNL/TM-13221, Oak Ridge National Laboratory, Oak Ridge, TN, USA, 1997.

- [10] G. A. Fischer, “Analysis Of The Pool Critical Assembly Benchmark Using RAPTOR-M3G, A Parallel Deterministic Radiation Transport Code,” in *PHYSOR 2010 — Advances in Reactor Physics to Power the Nuclear Renaissance*, (Pittsburgh, PA, USA), American Nuclear Society, May 2010.
- [11] G. Longoni and S. L. Anderson, “Reactor Dosimetry Applications Using Raptor-M3G: A New Parallel 3-D Radiation Transport Code,” in *Proceedings of the 13th International Symposium on Reactor Dosimetry*, (Akersloot, Netherlands), pp. 722–732, May 2008.
- [12] C. A. Edgar, “Improvements to the Pool Critical Assembly Benchmark using 3-D Discrete Ordinate Transport with Adaptive Difference,” Master’s thesis, Georgia Institute of Technology, Atlanta, GA, USA, 2013.
- [13] G. E. Sjoden, *PENTRAN: A Parallel 3-D SN Transport Code With Complete Phase Space Decomposition, Adaptive Differencing, and Iterative Solution Methods*. PhD thesis, Pennsylvania State University, State College, PA, USA, 1997.
- [14] V. G. Smith and B. P. Richardson, “Evaluation Of The Pool Critical Assembly Benchmark Using The TRANSFX Nuclear Analysis Software,” in *ANS MC2015 — Joint International Conference on Mathematics and Computation (M&C), Supercomputing in Nuclear Applications (SNA) and the Monte Carlo (MC) Method*, (Nashville, TN, USA), April 2015.
- [15] D. B. Jones *et al.*, “TRANSFX Theory Manual,” Tech. Rep. TWE-TFX-001-FM-016-001, TransWare Enterprises, Sycamore, IL, USA, 2015.
- [16] J. M. Risner *et al.*, “Production and Testing of the VITAMIN-B7 Fine-Group and BUGLE-B7 Broad-Group Coupled Neutron/Gamma Cross-Section Libraries Derived from ENDF/B-VII.0 Nuclear Data,” Tech. Rep. NUREG/CR-7045 (ORNL/TM-2011/12), Oak Ridge National Laboratory, Oak Ridge, TN, USA, 2011.
- [17] M. Matijević, D. Pevec, and K. Trontl, “Modeling of the ORNL PCA Benchmark Using SCALE6.0 Hybrid Deterministic-Stochastic Methodology,” *Science and Technology of Nuclear Installations*, vol. 2013, 2013.

- [18] Y. K. Lee, “Analysis Of The NRC PCA Pressure Vessel Dosimetry Benchmark Using TRIPOLI-4.3 Monte Carlo Code And ENDF/B-VI.4, JEF2.2 And IRDF-90 Libraries,” in *M&C 2003: Nuclear Mathematical and Computational Sciences: A Century in Review, A Century Anew*, (LaGrange Park, IL, USA), American Nuclear Society, 2003.
- [19] “SCALE 6: Standardized Computer Analyses for Licensing Evaluation Modular Code System for Workstations and Personal Computers, Including ORIGEN-ARP, RSICC Computer Code Collection CCC-750. Oak Ridge National Laboratory. Oak Ridge, TN, USA. August 2009.”
- [20] J. P. Both *et. al.*, "A Survey of TRIPOLI-4", 8th ICRS, pp. 373–377 (1994).
- [21] R. C. Little and R. E. Seamon, “Dosimetry/Activation Cross Sections for MCNP,” Tech. Rep. LA-UR-98-549, Los Alamos National Laboratory, Los Alamos, NM, USA, March 1984.
- [22] “International Reactor Dosimetry File 2002 (IRDF-2002),” Tech. Rep. Series No. 452, International Atomic Energy Agency, Vienna, Austria, 2006.
- [23] R. Capote, K. I. Zolotarev, V. G. Pronyaev, and A. Trkov, “Updating and Extending the IRDF-2002 Dosimetry Library,” *Journal of ASTM International*, vol. 9, pp. 1–9, April 2012.
- [24] J. M. Risner. Private Communication, 2015.
- [25] S. W. Mosher *et. al.*, “ADVANTG — An Automated Variance Reduction Parameter Generator,” Tech. Rep. ORNL/TM-2013/416, Oak Ridge National Laboratory, Oak Ridge, TN, USA, 2013.
- [26] N. Soppera, M. Bossant, and E. Dupont, “JANIS 4: An Improved Version of the NEA Java-based Nuclear Data Information System,” *Nuclear Data Sheets*, vol. 120, pp. 294–296, June 2014.
- [27] D. Wiarda, M. E. Dunn, D. E. Peplow, T. M. Miller, and H. Akkurt, “Development and Testing of ENDF/B-VI.8 and ENDF/B-VII.0 Coupled Neutron-Gamma Libraries for SCALE 6,” Tech. Rep. NUREG/CR-6990 (ONRL/TM-2008/047), Oak Ridge National Laboratory, Oak Ridge, TN, USA, February 2009.
- [28] “Calculational And Dosimetry Methods For Determining Pressure Vessel Neutron Fluence,” Reg. Guide 1.190, United States Nuclear Regulatory Commission, Washington, DC, USA, March 2001.

A Control & Regulating Rod Geometry

The details provided in this appendix are those received through private communication with the principal author of Reference 16. They are reproduced here to provide future analysts a clear and consistent modeling basis for the control and regulating rods.

There are three control rods and one regulating rod used in the PCA core. Critical rod positions are specified in Figure 1.5 of Reference 1; however, the critical positions given in this appendix are based on those used in Reference 16 and verified herein. The control rods are all inserted to the same axial position, with the bottom of the rod housing 13.17 cm above the core midplane elevation. The regulating rod is inserted such that the bottom of the rod is 5.89 cm above the core midplane elevation. The control rod consists of two cylindrical lead rods situated within an aluminum sleeve surrounded by B_4C enclosed within a racetrack-shaped aluminum housing. The regulating rod is strictly stainless steel 347. Dimensioned cross-sectional and elevation views of a typical control rod are shown in Figure 4 and similar views of the regulating rod are shown in Figure 5.

Tables

- I Experimental Reaction Rates Converted from Fission-Equivalent Flux Values (and Associated Uncertainties) from Reference 1
- II Experimental Reaction Rates (and Associated Uncertainties) Reproduced from Reference 7
- III Calculated Reaction Rates (and Associated Uncertainties) Using Packaged Dosimetry Cross Sections
- IV Calculated Reaction Rates (and Associated Uncertainties) Using IRDF-2002 Multi-group Dosimetry Cross Sections
- V Calculated Reaction Rates (and Associated Uncertainties) Using IRDFF v1.05 Dosimetry Cross Sections
- VI C/E Ratio Using Packaged Cross Sections versus Reference 1 Measurements
- VII C/E Ratio Using Packaged Cross Sections versus Reference 7 Measurements
- VIII C/E Ratio Using IRDF-2002 Cross Sections versus Reference 1 Measurements
- IX C/E Ratio Using IRDF-2002 Cross Sections versus Reference 7 Measurements
- X C/E Ratio Using IRDFF v.1.05 Cross Sections versus Reference 1 Measurements
- XI C/E Ratio Using IRDFF v1.05 Cross Sections versus Reference 7 Measurements

Table I: Experimental Reaction Rates Converted from Fission-Equivalent Flux Values (and Associated Uncertainties) from Reference 1

Location	Reaction Rate [rps per source neutron] ($\pm 1\sigma$ Uncertainty)					
	$^{27}\text{Al}(\text{n},\alpha)$		$^{58}\text{Ni}(\text{n},\text{p})$		$^{103}\text{Rh}(\text{n},\text{n}')$	
A1	5.55e-33	(1.0%)	6.35e-31	(1.4%)	4.06e-30	(1.0%)
A2	7.19e-34	(2.0%)	6.74e-32	(2.0%)	—	—
A3	3.16e-34	(1.0%)	2.52e-32	(1.4%)	—	—
A4	7.19e-35	(2.0%)	5.78e-33	(1.0%)	5.67e-32	(1.5%)
A5	2.89e-35	(2.2%)	2.28e-33	(1.8%)	3.19e-32	(5.0%)
A6	1.09e-35	(2.2%)	8.10e-34	(2.2%)	1.61e-32	(5.0%)
A7	—	—	—	—	—	—
Location	$^{115}\text{In}(\text{n},\text{n}')$		$^{238}\text{U}(\text{n},\text{f})$		$^{237}\text{Np}(\text{n},\text{f})$	
A1	1.06e-30	(1.0%)	—	—	8.71e-30	(6.2%)
A2	1.15e-31	(2.0%)	—	—	—	—
A3	3.76e-32	(1.0%)	—	—	2.98e-31	(6.3%)
A4	1.11e-32	(0.7%)	1.86e-32	(6.9%)	1.22e-31	(5.5%)
A5	5.22e-33	(1.5%)	8.36e-33	(6.8%)	6.80e-32	(5.7%)
A6	2.21e-33	(3.0%)	3.42e-33	(7.1%)	3.54e-32	(5.8%)
A7	—	—	—	—	9.51e-33	(9.2%)

Table II: Experimental Reaction Rates (and Associated Uncertainties) Reproduced from Reference 7

Location	Reaction Rate [rps per source neutron] ($\pm 1\sigma$ Uncertainty)					
	^{27}Al (n, α)		^{58}Ni (n,p)		^{103}Rh (n,n')	
A1	5.48e-33	(6.0%)	6.31e-31	(6.0%)	4.06e-30	(6.0%)
A2	7.16e-34	(6.0%)	6.72e-32	(6.0%)	4.50e-31	(6.0%)
A3	3.13e-34	(6.0%)	2.50e-32	(6.0%)	1.47e-31	(6.0%)
A4	7.15e-35	(6.0%)	5.69e-33	(6.0%)	5.67e-32	(6.0%)
A5	2.92e-35	(6.0%)	2.25e-33	(6.0%)	3.24e-32	(6.0%)
A6	1.12e-35	(6.0%)	7.99e-34	(6.0%)	1.67e-32	(6.0%)
A7	—	—	—	—	4.83e-33	(6.0%)
Location	^{115}In (n,n')		^{238}U (n,f)		^{237}Np (n,f)	
A1	1.05e-30	(6.0%)	—	—	—	—
A2	1.14e-31	(6.0%)	—	—	—	—
A3	3.68e-32	(6.0%)	5.91e-32	(5.8%)	3.05e-31	(5.8%)
A4	1.11e-32	(6.0%)	1.79e-32	(11.0%)	1.20e-31	(10.5%)
A5	5.20e-33	(6.0%)	7.88e-33	(10.9%)	6.56e-32	(11.2%)
A6	2.23e-33	(6.0%)	3.26e-33	(11.1%)	3.47e-32	(10.6%)
A7	6.43e-34	(6.0%)	8.65e-34	(4.9%)	9.60e-33	(7.3%)

Table III: Calculated Reaction Rates (and Associated Uncertainties) Using Packaged Dosimetry Cross Sections

Location	Reaction Rate [rps per source neutron] ($\pm 1\sigma$ Uncertainty)					
	$^{27}\text{Al}(\text{n},\alpha)$		$^{58}\text{Ni}(\text{n},\text{p})$		$^{103}\text{Rh}(\text{n},\text{n}')$	
A1	5.44e-33	(1.2%)	6.19e-31	(0.5%)	4.37e-30	(0.5%)
A2	7.17e-34	(2.1%)	6.67e-32	(0.6%)	5.05e-31	(0.4%)
A3	3.17e-34	(1.7%)	2.55e-32	(0.5%)	1.64e-31	(0.4%)
A4	7.19e-35	(2.7%)	5.65e-33	(0.7%)	6.07e-32	(0.3%)
A5	2.89e-35	(2.2%)	2.25e-33	(0.6%)	3.28e-32	(0.3%)
A6	1.06e-35	(3.1%)	8.22e-34	(1.3%)	1.68e-32	(0.5%)
A7	3.54e-36	(2.0%)	2.25e-34	(0.7%)	5.06e-33	(0.3%)
Location	$^{115}\text{In}(\text{n},\text{n}')$		$^{238}\text{U}(\text{n},\text{f})$		$^{237}\text{Np}(\text{n},\text{f})$	
A1	1.05e-30	(0.4%)	1.85e-30	(0.5%)	9.62e-30	(0.7%)
A2	1.15e-31	(0.4%)	2.00e-31	(0.5%)	1.13e-30	(0.5%)
A3	3.92e-32	(0.4%)	7.03e-32	(0.4%)	3.63e-31	(0.4%)
A4	1.14e-32	(0.4%)	1.87e-32	(0.4%)	1.31e-31	(0.3%)
A5	5.26e-33	(0.4%)	8.26e-33	(0.4%)	7.19e-32	(0.3%)
A6	2.28e-33	(0.7%)	3.43e-33	(0.9%)	3.70e-32	(0.5%)
A7	6.37e-34	(0.4%)	9.09e-34	(0.5%)	1.13e-32	(0.4%)

Table IV: Calculated Reaction Rates (and Associated Uncertainties) Using IRDF-2002 Multi-group Dosimetry Cross Sections

Location	Reaction Rate [rps per source neutron] ($\pm 1\sigma$ Uncertainty)					
	$^{27}\text{Al} (n, \alpha)$		$^{58}\text{Ni} (n, p)$		$^{103}\text{Rh} (n, n')$	
A1	5.39e-33	(1.2%)	6.40e-31	(0.5%)	4.36e-30	(0.5%)
A2	7.10e-34	(2.1%)	6.91e-32	(0.6%)	5.04e-31	(0.4%)
A3	3.14e-34	(1.7%)	2.64e-32	(0.5%)	1.64e-31	(0.4%)
A4	7.14e-35	(2.7%)	5.86e-33	(0.7%)	6.02e-32	(0.3%)
A5	2.87e-35	(2.2%)	2.33e-33	(0.6%)	3.22e-32	(0.3%)
A6	1.05e-35	(3.1%)	8.52e-34	(1.3%)	1.64e-32	(0.5%)
A7	3.51e-36	(2.0%)	2.34e-34	(0.7%)	4.92e-33	(0.3%)
Location	$^{115}\text{In} (n, n')$		$^{238}\text{U} (n, f)$		$^{237}\text{Np} (n, f)$	
A1	1.10e-30	(0.4%)	1.82e-30	(0.5%)	9.65e-30	(0.6%)
A2	1.21e-31	(0.4%)	1.97e-31	(0.5%)	1.12e-30	(0.4%)
A3	4.10e-32	(0.4%)	6.92e-32	(0.4%)	3.63e-31	(0.4%)
A4	1.20e-32	(0.4%)	1.85e-32	(0.4%)	1.31e-31	(0.3%)
A5	5.58e-33	(0.4%)	8.15e-33	(0.4%)	7.23e-32	(0.3%)
A6	2.43e-33	(0.7%)	3.39e-33	(0.9%)	3.73e-32	(0.5%)
A7	6.80e-34	(0.4%)	8.98e-34	(0.5%)	1.15e-32	(0.3%)

Table V: Calculated Reaction Rates (and Associated Uncertainties) Using IRDFF v1.05 Dosimetry Cross Sections

Location	Reaction Rate [rps per source neutron] ($\pm 1\sigma$ Uncertainty)					
	$^{27}\text{Al}(\text{n},\alpha)$		$^{58}\text{Ni}(\text{n},\text{p})$		$^{103}\text{Rh}(\text{n},\text{n}')$	
A1	5.28e-33	(1.2%)	6.40e-31	(0.5%)	4.36e-30	(0.5%)
A2	6.97e-34	(2.2%)	6.91e-32	(0.6%)	5.04e-31	(0.4%)
A3	3.08e-34	(1.8%)	2.64e-32	(0.5%)	1.64e-31	(0.4%)
A4	7.00e-35	(2.7%)	5.85e-33	(0.7%)	6.02e-32	(0.3%)
A5	2.82e-35	(2.2%)	2.33e-33	(0.6%)	3.22e-32	(0.3%)
A6	1.04e-35	(3.1%)	8.51e-34	(1.3%)	1.64e-32	(0.5%)
A7	3.45e-36	(2.0%)	2.33e-34	(0.7%)	4.91e-33	(0.3%)
Location	$^{115}\text{In}(\text{n},\text{n}')$		$^{238}\text{U}(\text{n},\text{f})$		$^{237}\text{Np}(\text{n},\text{f})$	
A1	1.09e-30	(0.4%)	1.82e-30	(0.5%)	9.60e-30	(0.7%)
A2	1.20e-31	(0.4%)	1.96e-31	(0.5%)	1.12e-30	(0.5%)
A3	4.08e-32	(0.4%)	6.91e-32	(0.4%)	3.63e-31	(0.4%)
A4	1.19e-32	(0.4%)	1.83e-32	(0.4%)	1.31e-31	(0.3%)
A5	5.55e-33	(0.4%)	8.09e-33	(0.4%)	7.23e-32	(0.3%)
A6	2.42e-33	(0.7%)	3.36e-33	(0.9%)	3.74e-32	(0.5%)
A7	6.77e-34	(0.4%)	8.89e-34	(0.5%)	1.15e-32	(0.4%)

Table VI: C/E Ratio Using Packaged Cross Sections versus Reference 1 Measurements

Location	$^{27}\text{Al}(\text{n},\alpha)$	$^{58}\text{Ni}(\text{n},\text{p})$	$^{103}\text{Rh}(\text{n},\text{n}')$	$^{115}\text{In}(\text{n},\text{n}')$	$^{238}\text{U}(\text{n},\text{f})$	$^{237}\text{Np}(\text{n},\text{f})$	Average
A1	0.98	0.97	1.08	0.99	—	1.10	1.02
A2	1.00	0.99	—	1.01	—	—	1.00
A3	1.00	1.01	—	1.04	—	1.22	1.07
A4	1.00	0.98	1.07	1.03	1.00	1.07	1.03
A5	1.00	0.99	1.03	1.01	0.99	1.06	1.01
A6	0.98	1.02	1.05	1.03	1.01	1.04	1.02
A7	—	—	—	—	—	1.19	1.19
Average	0.99	0.99	1.06	1.02	1.00	1.11	1.05

Table VII: C/E Ratio Using Packaged Cross Sections versus Reference 7 Measurements

Location	$^{27}\text{Al}(\text{n},\alpha)$	$^{58}\text{Ni}(\text{n},\text{p})$	$^{103}\text{Rh}(\text{n},\text{n}')$	$^{115}\text{In}(\text{n},\text{n}')$	$^{238}\text{U}(\text{n},\text{f})$	$^{237}\text{Np}(\text{n},\text{f})$	Average
A1	0.99	0.98	1.08	1.00	—	—	1.01
A2	1.00	0.99	1.12	1.01	—	—	1.03
A3	1.01	1.02	1.11	1.06	1.19	1.19	1.10
A4	1.01	0.99	1.07	1.03	1.04	1.09	1.04
A5	0.99	1.00	1.01	1.01	1.05	1.10	1.03
A6	0.95	1.03	1.01	1.02	1.05	1.07	1.02
A7	—	—	1.05	0.99	1.05	1.18	1.07
Average	0.99	1.00	1.06	1.02	1.08	1.13	1.04

Table VIII: C/E Ratio Using IRDF-2002 Cross Sections versus Reference 1 Measurements

Location	$^{27}\text{Al}(\text{n},\alpha)$	$^{58}\text{Ni}(\text{n},\text{p})$	$^{103}\text{Rh}(\text{n},\text{n}')$	$^{115}\text{In}(\text{n},\text{n}')$	$^{238}\text{U}(\text{n},\text{f})$	$^{237}\text{Np}(\text{n},\text{f})$	Average
A1	0.97	1.01	1.07	1.04	—	1.11	1.04
A2	0.99	1.03	—	1.06	—	—	1.03
A3	1.00	1.05	—	1.09	—	1.22	1.09
A4	0.99	1.01	1.06	1.08	0.99	1.07	1.03
A5	0.99	1.02	1.01	1.07	0.98	1.06	1.02
A6	0.97	1.05	1.02	1.10	0.99	1.05	1.03
A7	—	—	—	—	—	1.21	1.21
Average	0.99	1.03	1.04	1.07	0.99	1.12	1.06

Table IX: C/E Ratio Using IRDF-2002 Cross Sections versus Reference 7 Measurements

Location	$^{27}\text{Al}(\text{n},\alpha)$	$^{58}\text{Ni}(\text{n},\text{p})$	$^{103}\text{Rh}(\text{n},\text{n}')$	$^{115}\text{In}(\text{n},\text{n}')$	$^{238}\text{U}(\text{n},\text{f})$	$^{237}\text{Np}(\text{n},\text{f})$	Average
A1	0.98	1.01	1.08	1.05	—	—	1.03
A2	0.99	1.03	1.12	1.06	—	—	1.05
A3	1.00	1.06	1.12	1.11	1.17	1.19	1.11
A4	1.00	1.03	1.06	1.08	1.03	1.09	1.05
A5	0.98	1.04	0.99	1.07	1.03	1.10	1.04
A6	0.94	1.07	0.98	1.09	1.04	1.08	1.03
A7	—	—	1.02	1.06	1.04	1.20	1.08
Average	0.98	1.04	1.05	1.07	1.06	1.13	1.06

Table X: C/E Ratio Using IRDFF v.1.05 Cross Sections versus Reference 1 Measurements

Location	$^{27}\text{Al}(\text{n},\alpha)$	$^{58}\text{Ni}(\text{n},\text{p})$	$^{103}\text{Rh}(\text{n},\text{n}')$	$^{115}\text{In}(\text{n},\text{n}')$	$^{238}\text{U}(\text{n},\text{f})$	$^{237}\text{Np}(\text{n},\text{f})$	Average
A1	0.95	1.01	1.07	1.03	—	1.10	1.03
A2	0.97	1.03	—	1.05	—	—	1.02
A3	0.98	1.05	—	1.08	—	1.22	1.08
A4	0.97	1.01	1.06	1.08	0.98	1.07	1.03
A5	0.97	1.02	1.01	1.06	0.97	1.06	1.02
A6	0.95	1.05	1.02	1.09	0.98	1.05	1.02
A7	—	—	—	—	—	1.21	1.21
Average	0.97	1.03	1.04	1.07	0.98	1.12	1.06

Table XI: C/E Ratio Using IRDFF v1.05 Cross Sections versus Reference 7 Measurements

Location	$^{27}\text{Al}(\text{n},\alpha)$	$^{58}\text{Ni}(\text{n},\text{p})$	$^{103}\text{Rh}(\text{n},\text{n}')$	$^{115}\text{In}(\text{n},\text{n}')$	$^{238}\text{U}(\text{n},\text{f})$	$^{237}\text{Np}(\text{n},\text{f})$	Average
A1	0.96	1.01	1.08	1.04	—	—	1.02
A2	0.97	1.03	1.12	1.05	—	—	1.04
A3	0.99	1.06	1.12	1.11	1.17	1.19	1.11
A4	0.98	1.03	1.06	1.08	1.03	1.09	1.05
A5	0.96	1.04	0.99	1.07	1.03	1.10	1.03
A6	0.92	1.06	0.98	1.09	1.03	1.08	1.03
A7	—	—	1.02	1.05	1.03	1.20	1.08
Average	0.96	1.04	1.05	1.07	1.06	1.13	1.05

Figures

- 1 Plan View of ORNL PCA PVWBF Model
- 2 Detailed Plan View of ORNL PCA Control Rod Model And Surrounding Fuel Assembly Geometry
- 3 IRDF-2002 Multi-Group Dosimetry Microscopic Cross Sections
- 4 Control Rod Dimensions (Plan View, Left, Through Break In Elevation View, Right)
- 5 Regulating Rod Dimensions (Plan View, Left, Through Break In Elevation View, Right)

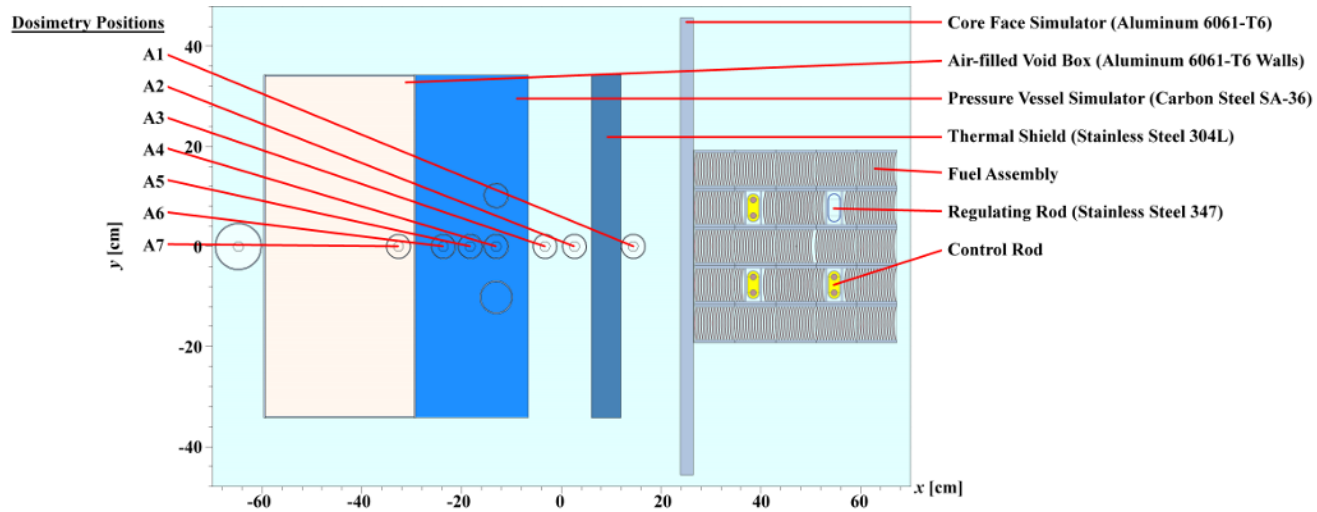


Figure 1: Plan View of ORNL PCA PVWBF Model

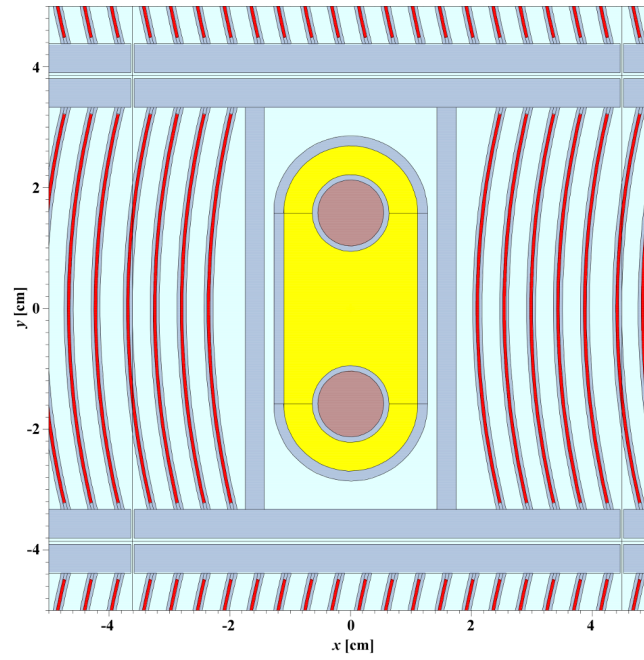


Figure 2: Detailed Plan View of ORNL PCA Control Rod Model And Surrounding Fuel Assembly Geometry

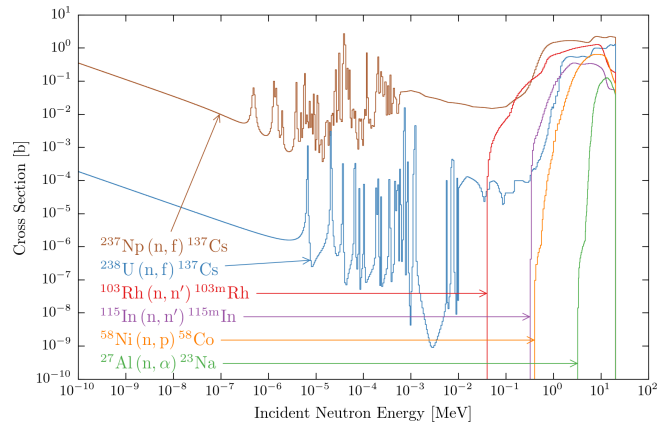


Figure 3: IRDF-2002 Multi-Group Dosimetry Microscopic Cross Sections

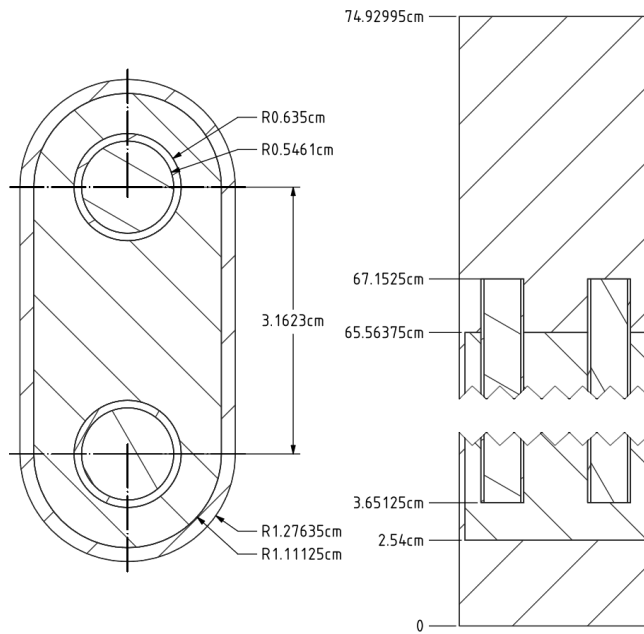


Figure 4: Control Rod Dimensions (Plan View, Left, Through Break In Elevation View, Right)

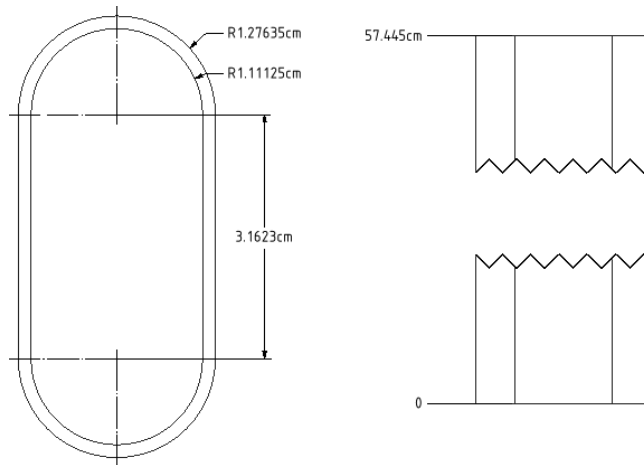


Figure 5: Regulating Rod Dimensions (Plan View, Left, Through Break In Elevation View, Right)